AIAA JOURNAL
Vol. 40, No. 12, December 2002

Control of an Oblique Shock/Boundary-Layer Interaction with Aeroelastic Mesoflaps

Derek Gefroh,* Eric Loth,† Craig Dutton,‡ and Stephen McIlwain§
University of Illinois at Urbana–Champaign, Urbana, Illinois 61801

Aeroelastic mesoflaps for recirculating transpiration have been investigated in an effort to control shock/boundary-layer interactions (SBLIs) through passive cavity recirculation. The mesoflap concept utilizes a matrix of small flaps covering an enclosed cavity that are designed to undergo local aeroelastic deflection to achieve proper mass bleed or injection when subjected to gasdynamic pressure loading. Experiments were performed to investigate the applicability of the mesoflap concept for oblique shock interaction by employing shadowgraph flow visualizations, surface pressure measurements, and mean and fluctuating velocity measurements, along the spanwise midplane of the shock intersection. The experiments were conducted in a Mach 2.41 supersonic wind tunnel operating at a unit Reynolds number of 57×10^6 m^{-1}. With the thickest mesoflap arrays in place, the leading shock formed at the location of the first flap and the boundary-layer thickness at shock impingement was greater due to flow injection through the upstream flaps. However, the thinnest mesoflap arrays yielded a somewhat reduced boundary-layer thickness downstream of the interaction as a result of the tangential bleeding by the last flaps. Stagnation pressure profiles for the thinnest arrays also showed improved recovery downstream of the SBLI as compared to the solid-wall case. However, further study is needed to investigate three-dimensional effects and to determine whether this control strategy provides significant performance improvements for flow conditions more consistent with actual inlets.

Introduction

Shock/Boundary-Layer Interaction Flows

FOR both internal and external supersonic aerodynamics, the interaction between shock waves and turbulent boundary layers can be critical because the strong adverse pressure gradient caused by an impinging shock can cause the outgoing boundary layer to be severely distorted or even separated. A detailed discussion of the flow physics of such interactions is given by Delery and Bur,[1] and a detailed investigation of the mean flow and turbulence properties of transonic (normal) shock/boundary-layer interactions (SBLIs) was conducted by Delery[2] using two-component laser Doppler velocimetry (LDV). In the latter study, the cases of separated flow yielded a downstream boundary-layer thickness δ that was 10 times that of the incoming value and were associated with large turbulence generation (primarily in the streamwise velocity component).

In general, oblique-shock interactions can be classified as either impinging-shock cases or ramp/body-generated shock cases. Settles and Dodson[3] reviewed experimental studies on supersonic and hypersonic SBLI flows to identify suitable candidates to guide code validation efforts. Although their literature search uncovered a multitude of relevant articles on ramp/body-generated SBLI flows, they found that high-quality experimental data on impinging oblique SBLIs were relatively scarce. Hamed and Kumar[4] also examined the conditions for incipient separation due to SBLI of both compression corners and impinging oblique shocks. They reported that the shock-induced flow separation angle increases with increasing Mach number, but the effect of Reynolds number on incipient separation is still uncertain because different studies have shown opposing trends. However, there have only been a few experimental studies on impinging oblique-shock interactions and none that have employed noninstrusive diagnostics to measure the downstream velocity and turbulence properties.

Bleed and Injection Studies

The deleterious effects of boundary-layer separation and flow unsteadiness caused by shock interaction is most typically reduced by using bleed in the immediate vicinity of the shock front. Several experimental and numerical studies have been conducted to determine the ideal bleed location in an effort to reduce the bleed-flow rates currently used in supersonic inlets. Hamed et al.[5] report that there are disagreements among the conclusions drawn from experimental studies as to whether the ideal bleed location is upstream of the shock, within the interaction region, or downstream. In their numerical study on oblique-shock interactions at $M = 2.96$, a downstream placement of the normal slots appeared to minimize δ^* and θ of the outgoing boundary layer for low bleed mass flow rates, as did the lowest slot angle (20 deg).

Upstream tangential injection is another method that has been demonstrated to reduce separation and lead to fuller velocity profiles after shock impingement. Donovan[6] conducted experimental and computational studies at Mach 3.4 for an oblique shock impinging on a turbulent boundary layer at various angles. For the separated cases, a tangential injection jet $0.33\delta_0$ high, placed between 5.5 and $7.1\delta_0$ upstream of inviscid shock impingement, yielded substantial improvement in static pressure recovery and boundary-layer velocity deficit.

Recirculating Flow Control Studies

An alternative to bleeding is recirculating (passive) flow control of the SBLI, which may be important for transonic aerodynamics, as well as supersonic engine inlets.[7] In this technique, the pressure difference across the shock is communicated through a porous medium covering a cavity, thereby causing transpiration to occur without active suction. The result is injection upstream of the interaction, effectively to reduce the shock strength and suction downstream to bleed off the boundary layer, thereby reducing separation. The concept of using recirculating flow to control SBLIs was first proposed by Bushnell and Whitcomb (as reported by Bahi[8]) in 1979 for supercritical airfoils and was experimentally demonstrated and published by Bahi et al. in 1983 (Ref. 9). Since that time, a substantial

Received 19 April 2001; revision received 5 June 2002; accepted for publication 22 July 2002.

*Graduate Research Assistant, Department of Aeronautical and Astronautical Engineering. Student Member AIAA.

†Professor, Department of Aeronautical and Astronautical Engineering, 104 South Wright Street. Associate Fellow AIAA.

‡W. Grafton and Lillian B. Wilkins Professor, Department of Mechanical and Industrial Engineering. Associate Fellow AIAA.

§Senior Research Scientist, Department of Aeronautical and Astronautical Engineering. Member AIAA.

amount of research investigating the applicability of this passive control concept on transonic airfoils ($M < 1.4$) has been conducted, both experimentally and numerically. The concept is also attractive for high-speed inlets; because there is no net mass removal, bleed ducting and dumping systems may be eliminated. In particular, the Boeing Company and Lockheed Martin have both noted that a bleedless inlet can allow dramatic improvements in overall performance of aircraft designed for supersonic cruise conditions.[10]

The porous media tested to date (experimentally and numerically) have primarily focused on normal-shock interactions using holes and slots, both slanted and normal.[5,11,12] Experiments by Raghunathan and McIlwain[12] examined normal-shock SBLIs on a NACA 14% thick airfoil at Mach numbers of 1.20, 1.27, 1.30, and 1.34. Both normal holes and forward-facing holes were tested, each case with hole diameters of $2\delta^*$ and a porosity of 2.14%. The study found that the interaction length was increased, and the normal shock was split into two shock waves, which indicates increased communication across the interaction region. In addition, this configuration resulted in an increase of the boundary-layer thickness and shape factor compared to that of the solid-wall case. However, the overall stagnation pressure loss was reduced by 10%, which is attributed to the weakening of the shock system resulting from the upstream injection. Recirculating flow control studies for normal SBLIs by Bur et al.[13,14] were conducted at Mach 1.34 with four different plates, each with a surface porosity of 5.67%. Again, the flow control increased the downstream boundary-layer displacement thickness and momentum thickness, but still achieved an overall reduction in drag coefficient of 4% as compared to the solid-wall case.

McCormick[15] also conducted an experimental study of the recirculating flow and vortex generator techniques to control transonic normal-shock SBLI flows. With the vortex generators, the separated region was reduced in length (by one-half). Whereas the recirculating cavity had the opposite effect for separation length, the total pressure recovery was significantly increased as compared to the baseline and vortex generator experiments. Computations by Gibson et al.[16] verified this result and showed a trend that higher porosity leads to superior pressure recovery. Finally, some work on the use of recirculating control systems for supersonic inlet flow was performed by Rolston and Raghunathan,[17] who showed that the location of the normal preentry shock could be controlled by the recirculating system and was accompanied by an increase in stagnation pressure. However, the recirculating technique has not been adopted for transonic airfoils or supersonic inlets, primarily due to aerodynamic losses associated with hole geometry,[14] and increased drag penalties for no-shock or off-design flow conditions due to plate roughness.[18] Also note that very little research has been conducted on the passive control of oblique SBLIs, including no known experimental efforts to date.[19]

Mesoflap Concept

The goal of the mesoflap concept is to reduce or eliminate flow separation caused by SBLIs and increase the total pressure recovery, thereby improving the resulting downstream boundary-layer characteristics. The concept consists of a matrix of mesoflaps covering an enclosed cavity, as shown in Figs. 1a and 1b, and an experimentally tested mesoflap array and its spars, as shown in Figs. 1c and 1d. Each of the flaps is rigidly fixed over a small portion of its upstream end (by the spars shown in Fig. 1d) but can aeroelastically deflect at its downstream end based on the pressure difference between the supersonic flow above and the subsonic cavity flow below. Under no-shock conditions, that is, subsonic flow, the pressures above and below the flaps are nearly equal, such that no transpiration is induced (Fig. 1a). Because the surface is nearly aerodynamically smooth for the case of no-shock impingement, the roughening of the surface caused by conventional transpiration holes or slots is reduced.

Figure 1b shows the mesoflap system with an oblique shock impinging on the mesoflaps, which induces a strong streamwise pressure variation. The nearly constant cavity pressure will lie somewhere between the low pressure of the incoming preshocked flow and the high pressure of the outgoing shocked flow. Consequently, the flaps upstream of the impingement location will deflect upward, allowing flow injection angled into the boundary layer, and the flaps

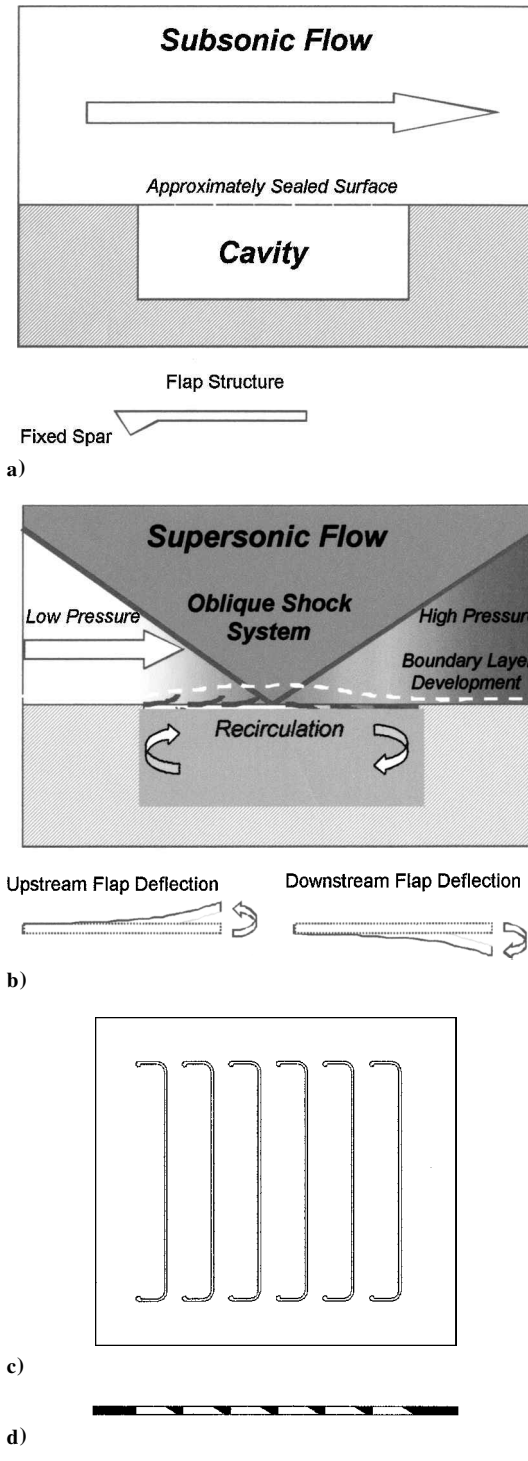

Fig. 1 Mesoflap system for a) subsonic flow and b) supersonic flow with impinging oblique shock; view of experimentally tested mesoflap system viewed c) from above and d) from side showing spars.

downstream will deflect downward to allow angled bleed from the boundary layer into the cavity. Therefore, the flaps deflect locally in a cantilever mode due to the surrounding aerodynamic pressure distribution to achieve appropriately angled bleed and injection, that is, they are aeroelastically "smart." The mesoflap system can easily be designed to accommodate variations in both streamwise position and shock sweep angle by constructing the flaps in a two-dimensional matrix in both the spanwise and streamwise directions (Fig. 2).

The objective of the present study was to conduct experimental measurements of the mesoflap flowfield for different flap thicknesses because previous efforts were purely computational.[20] In particular, the structural performance of the flaps (ability to withstand the SBLI) and the transpiration flow control performance

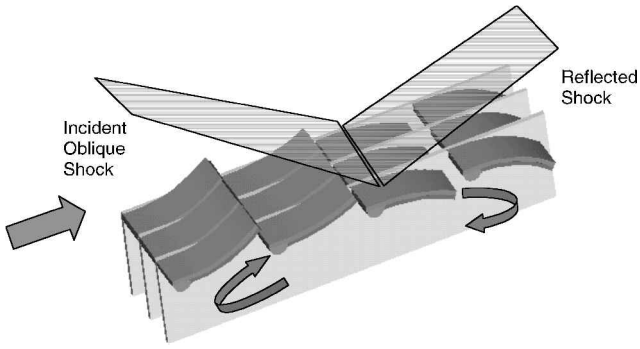

Fig. 2 Three-dimensional view of meosflap concept.

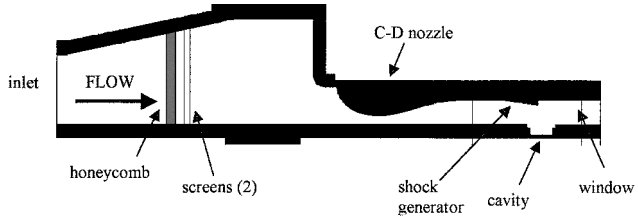

Fig. 3 Supersonic wind-tunnel schematic where flow is left to right.

(whether it harms or improves the outgoing boundary-layer characteristics and whether it increases or decreases stagnation pressure recovery) were investigated.

Experimental Facility and Methods

Flow Facility

The experiments reported here were conducted in a continuous-flow supersonic wind tunnel with a two-dimensional planar cross section (a side view is shown in Fig. 3), located in the Gas Dynamics Laboratory at the University of Illinois at Urbana–Champaign (UIUC). High-pressure desiccated air enters the inlet, which houses a flow-conditioning system consisting of honeycomb cells followed by two mesh screens. The test section width is constant from the exit of the nozzle to the exit of the tunnel at 50.8 mm. The nozzle is designed for an exit plane Mach number of 2.45 with an exit height of 50.8 mm and throat height of 18.4 mm. However, the Mach number farther downstream and just above the incoming boundary layer to the mesoflap arrays was measured to be 2.41 due to the boundary-layer growth. Removable fused-silica windows in the tunnel side walls provide full optical access to the test section. The windows offer a viewable area of 18.5 by 3.9 cm. The freestream unit Reynolds number is 57×10^6 m^{-1}. A more detailed description of the wind-tunnel facility, its design evolution, and the air delivery system is given by Gefroh.[21]

An 8-deg shock generator is installed on the upper wall of the test section to produce an oblique shock that impinges on the lower wall of the wind tunnel. Together, the incident and reflected shocks generate a pressure rise of 2.5–1. A cavity covered by an array of mesoflaps is centered at the oblique shock impingement location. The cavity is 44.5 mm long and 19.1 mm deep and spans the entire width (50.8 mm) of the tunnel test section. The lower wall with the cavity is removable and can be replaced with a solid wall to perform no-bleed baseline studies. At the ramp start location, the boundary layer on the lower wall is fully turbulent with a 99.5% thickness of 4.0 mm and a momentum thickness of 0.30 mm, where $Re_\theta = 1.7 \times 10^4$.

Mesoflap Design

Four different thicknesses of mesoflap arrays, each comprising six individual mesoflaps, were used in the present study. The mesoflap system consists of a steel frame with spanwise-running support spars, to which a nickel–titanium (nitinol) flap array is epoxied. The mesoflap array thickness was varied between 50 and 150 μm, yielding a corresponding change in flap stiffness and deflection once subjected to shock-induced aerodynamic loads. Each flap spanned three-quarters of the tunnel width and had a streamwise length of 4.63 mm. (The six-flap array is shown from above in Fig. 1c.) To prevent flow blockage into the cavity, the leading edge of each supporting steel spar (Fig. 1d) was machined to a triangular shape (30 deg to the streamwise direction). The design evolution of the mesoflap system, along with detailed schematics, is given by Gefroh.[21]

Experimental Techniques

The efficacy of the mesoflap system in controlling SBLI flows was evaluated using shadowgraph flow visualizations, surface pressure distributions, and LDV measurements in the evolving boundary layer. Single-frame shadowgraph photography was used to visualize qualitatively the oblique shock waves, expansion fans, and boundary-layer turbulence structure. Static pressure taps were placed along the spanwise centerline of the lower wall of the tunnel and along the bottom wall of the cavity, with a streamwise spacing of 3.18 mm. Although no spanwise measurements were conducted in this study, similar experiments on a solid-wall case and a mesoflap case with an oblique-shock interaction of comparable strength were conducted at NASA John H. Glenn Research Center at Lewis Field (GRC). The GRC experiments employed a Mach 2 wind tunnel with a 12:1 ratio of channel width to incoming boundary-layer thickness (the ratio was 19:1 for the present studies) and obtained surface flow visualizations.[10] In general, the flow separation regions in the GRC experiments for both the solid-wall and mesoflap cases were found to be approximately two-dimensional for the majority of the span and especially along the centerline (expected due to symmetry). However, significant side-wall interaction effects appear to be present near the walls (corresponding roughly to the outer 20% portions of the tunnel width) and, in addition, significant three dimensionality was noted near the streamwise edges of the upstream mesoflaps.[10]

LDV has been used extensively in the past for supersonic flows at UIUC, including application to SBLI flows.[22,23] The present study utilized a one-component LDV setup to allow high spatial resolution near the wall and a Bragg cell optoacoustical frequency-shifting method to resolve flow direction ambiguity in the separated region near the wall. Artificial seeding was employed in the LDV investigation using a TSI six-jet silicone oil atomizer. The polydispersed silicone oil droplets have a mean diameter of approximately 0.8 μm and have been found in previous studies to follow turbulent flow fluctuations of frequencies of at least 30 kHz and, perhaps, even above 200 kHz.[24,25] The silicone droplets were injected into the stagnation chamber just after the flow conditioning system and upstream of the nozzle throat. For the present investigation, the ensemble of instantaneous streamwise velocity measurements at each spatial location consisted of 4096 realizations. The overall maximum uncertainties in the measurements of the mean velocity and streamwise turbulence intensity are 2.0% and 0.79% of the maximum velocity, respectively.[21]

Results and Discussion

Mesoflap Aeroelastic Behavior

Because flap deflection is theoretically proportional to streamwise flap length cubed and inversely proportional to flap thickness cubed, the flap geometry is crucial to the performance of the mesoflap system. In general terms, the mesoflap arrays deflected under aeroelastic loads as anticipated, that is, the flaps upstream of impingement deflected up and those downstream deflected down to allow for angled bleed. It was found that the flaps that deflected the largest amount were the leading and trailing flaps, whereas the middle flaps remained relatively undeflected during the experiments (due to zero-pressure difference across the upper and lower surfaces at midcavity). The maximum flap deflection of the thinnest nitinol array (50.8-μm thick) was approximately 30 deg under the aerodynamic loading conditions of the present experiments.

Shadowgraph Flow Visualizations

The typical features of an oblique-shock SBLI are identifiable in Fig. 4a, which shows the flow over the solid wall at the location of shock impingement. The flow direction is from left to right. The incident shock clearly impinges on the lower wall and reflects, and several weak gasdynamic waves also emanate upward from the interaction region downstream of the primary reflected shock. Note

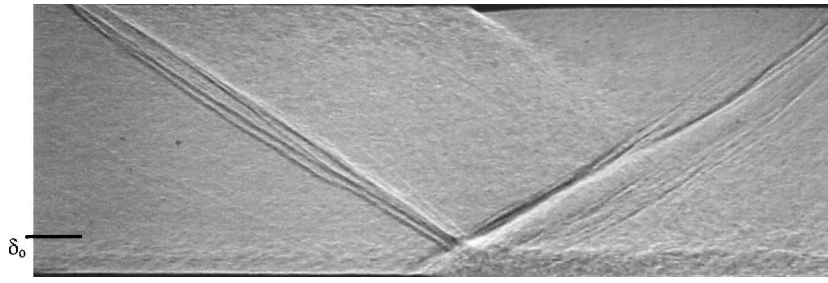

a) Solid wall (reference case)

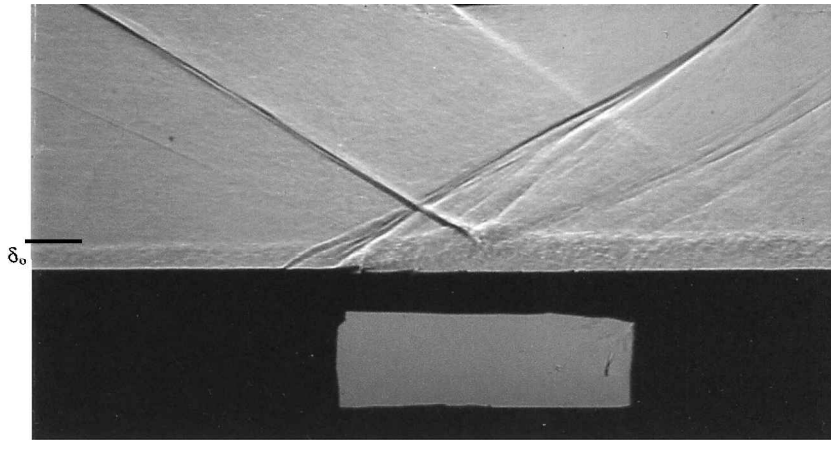

b) Nitinol mesoflap array (76.2 μm)

Fig. 4 SBLI shadowgraphs.

that the impinging shock wave shows some variation in thickness, indicating unsteadiness of the impinging wave, which was noted in many cases. Substantial thickening of the boundary layer near the impingement point is clearly evident; the boundary-layer thickness 35 mm downstream of shock impingement was estimated at around 5 mm. Numerous authors have described the aforementioned features of solid-wall SBLIs (for example, see Seddon[26]). The expansion fan emanating from the downstream tip of the shock-generator wedge can be seen entering the top of the shadowgraph and impacting the boundary-layer edge approximately 44 mm ($11\delta_0$) downstream of shock impingement. The reflected shock curves upward slightly as it passes through the waves in the expansion fan.

Shadowgraph images were also obtained for four different thicknesses of nitinol mesoflap arrays. A typical image of the SBLI with a 76.2-μm-thick flap array is shown in Fig. 4b. The leading oblique shock associated earlier with the rapid thickening of the wall boundary layer in the solid-wall case was located further upstream at a position over the first flap. This is clear evidence of the upward deflection of the upstream flaps, coupled with flow injection from this flap location, and is typical of other work on passive control of SBLIs.[14,27] The incident shock remained in the same location as for the solid-wall case. Expansion waves were also observed downstream of the shock impingement location; this and other features can also be noted in the aeroleastic simulations reported by Wood et al.[20]

A substantial increase in boundary-layer thickness is observed through the initial portion of the interaction region, which is indicative of much higher rates of mass injection than for the thicker flap arrays tested. Estimates of the boundary-layer thickness 13 mm downstream of the cavity were approximately 5 mm, which is about the same thickness as the solid-wall boundary layer at this location.

A feature that becomes more prominent for thinner flaps (Fig. 4b) is the trailing compression wave that originates at the downstream end of the cavity. The trailing shock forms when the angled bleed flow occurring over the last flap is redirected to the horizontal (over the downstream wall) by the rigid structure following the mesoflaps. Examination of other cases shows that this trailing shock strength was consistently increased as the flap thickness was reduced. The streamwise location of the intersection between the first wave of the expansion fan from the shock generator and the trailing shock ($8.7\delta_0$ downstream of shock impingement) is where many of the detailed measurements of the outgoing boundary-layer characteristics were made. At this location, it is reasonable to assume that the static pressure across the boundary layer is constant, which, thus, enables an appropriate determination of the stagnation pressure profiles from the measured velocity profiles. The expansion fan interacts with the boundary layer approximately $11\delta_0$ downstream of impingement, beyond which a constant static pressure assumption across the boundary layer is invalid.

Wall Static Pressure Results

The centerline wall static pressure distribution, normalized by the upstream stagnation pressure, is shown in Fig. 5 for the baseline solid wall and with the mesoflap arrays installed; x_0 corresponds to the middle of the cavity and is also the approximate shock impingement location, based on extending the impinging shock seen in the shadowgraphs to the wall. The reference boundary layer thickness δ_0 is 4 mm. The pressure data are repeatable over several separate trial runs.

The solid-wall pressure distribution is nearly constant upstream of the shock impingement, and the magnitude is consistent with that for Mach 2.45 approach flow. As the impending shock impingement is communicated upstream through the subsonic region near the wall, the boundary layer thickens and the pressure slowly increases in response to the weak compression waves that are generated. The shock impinges approximately $2.2\delta_0$ upstream of the location predicted by inviscid analysis and is distributed over approximately 20 mm ($5\delta_0$), which is typical of SBLIs. The pressure downstream of the interaction is nearly constant until it decreases with the impingement of the expansion fan produced at the tip of the shock generator. Several authors[14,15,28] have used centerline static pressure taps to ascertain the locations of separation and reattachment by inflections in the static pressure distribution. Unfortunately, the streamwise spacing of the pressure taps in the present study (3.18 mm) provided inadequate spatial resolution for conclusive determination of the separation characteristics based on this criterion. Therefore, the shadowgraphs and the LDV results (to be discussed later) were primarily used to indicate qualitatively the locations of

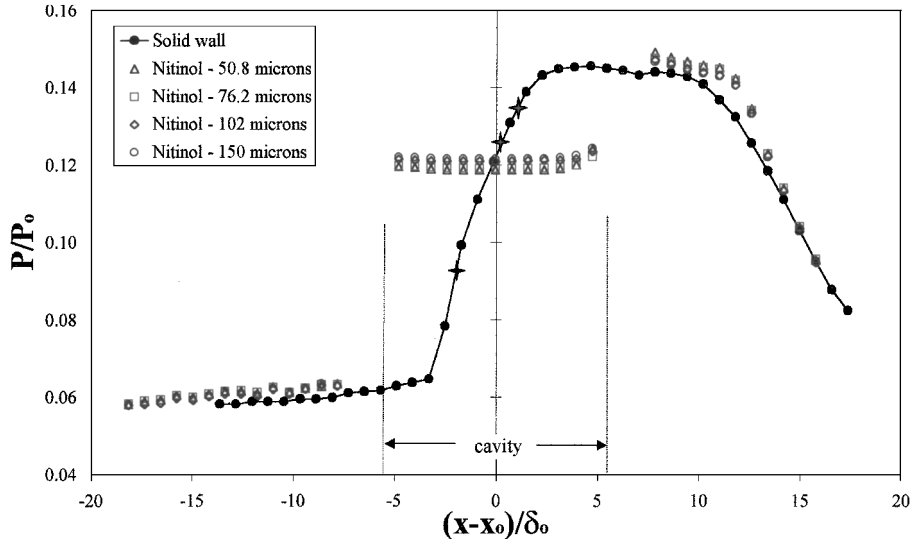

Fig. 5 Streamwise centerline surface pressure measurements for SBLI with different thicknesses of nitinol mesoflap arrays; note that the pressures in the cavity region for the mesoflap cases are at the bottom of the cavity, whereas there is no cavity for the solid-wall case (+ indicates the locations of separation, the onset of reattachment, and the reattachment compression).

separation (approximately $2\delta_0$ upstream of impingement), the onset of reattachment (near shock impingement), and the effect of reattachment compression (approximately $1\delta_0$ downstream of impingement); these three points are noted as three stars in Fig. 5. This yields an estimate of a $3\delta_0$–long separation region.

With the nitinol mesoflap arrays installed, the pressure rise preceding oblique-shock impingement is shifted upstream, irrespective of mesoflap thickness. This offset is due to small differences in the cross-sectional area that occurred when the wind tunnel was taken apart and reassembled between the solid-wall condition and the mesoflap condition. Note that a solid-wall insert case was also considered using the same tunnel assembly as for the mesoflap cases and yielded identical upstream pressure values as for the mesoflap cases. However, this case was not chosen to be the baseline because it had small surface perturbations at the insert edges as compared to the case for which the entire lower wall was a single surface, such that the latter case was felt to be more appropriate for comparison. Also note that the slight pressure rise upstream of shock impingement for both the solid-wall and the mesoflap cases is attributed to slight decreases in Mach number associated with boundary-layer growth in the constant cross-section wind tunnel.

In the flap region, the pressure at the bottom of the cavity is relatively constant for all mesoflap thicknesses, with a slight increase at the downstream end. This constant cavity pressure result is consistent with the study by Bur et al.[14] of normal SBLIs with porous plates. Note, however, that the cavity pressure is not simply equal to the average of the pressures upstream and downstream of the SBLI. Rather, the lambda shock created by flow injection at the first flap compresses the flow, resulting in a cavity pressure 12% higher than the average of the pressures before and after shock impingement. This result implies that the upstream flaps deflect upward more than the downstream flaps deflect downward. Notably, the cavity pressure for the two thinnest mesoflaps is slightly less than the pressure for the two thickest cases. (The possible reasons for this behavior are unclear.)

Downstream of the interaction, the static pressure for all mesoflap thicknesses is clearly higher than that for the solid-wall case, especially for the two thinnest flap arrays (50.8 and 76.2 μm). This indicates a somewhat higher downstream static pressure recovery as compared to the baseline solid-wall model.

Velocity Measurements

LDV measurements were obtained for the solid-wall baseline case and a variety of nitinol flap array thicknesses. Data obtained from the velocity traverses were used to calculate the boundary-layer integral parameters and streamwise turbulence intensity profiles to determine the state of the outgoing boundary layer. A complete flowfield map of the mean streamwise velocity and streamwise turbulence intensity characteristics for the solid wall was made upstream, downstream, and within the SBLI. An experimental curve fit based on the compressible, turbulent boundary-layer velocity profile of Sun and Childs[29] was used to determine the incoming boundary-layer thickness (typically δ_{99}) and skin-friction coefficient. The boundary-layer thickness determined by the curve fit was in agreement with the transverse position where the magnitudes of the higher-order moments of the streamwise velocity fluctuations (skewness and kurtosis) increased dramatically, due to intermittency at the boundary-layer edge. The impingement of the expansion fan on the boundary layer at approximately $11\delta_0$ downstream of shock impingement makes it difficult to establish a true boundary-layer thickness beyond that location. The remaining boundary-layer parameters (δ^*, θ, and H_i) were calculated directly from the experimental data using standard trapezoid-rule integration.

Solid-Wall Baseline Study

The streamwise velocity characteristics of the entire flowfield for the no-bleed, solid-wall baseline case were mapped with 20 streamwise-spaced boundary-layer profiles on the spanwise midplane of the tunnel. Five of the mean velocity profiles before and after shock impingement are presented in Fig. 6, including the reference incoming profile. In Fig. 6 and as shown subsequently, $x^* = (x - x_0)/\delta_0$ is the streamwise distance downstream of shock impingement x_0, normalized by the incoming boundary layer thickness ($\delta_0 = 4.0$ mm). The streamwise velocities are normalized by the incoming freestream velocity ($U_0 = 569$ m/s).

The effects of an impending, discrete adverse pressure gradient have been shown for locations as early as $3\delta_0$ upstream of shock impingement.[21] At this location, the boundary layer thickens substantially and the profile is no longer characteristic of a zero-pressure-gradient, turbulent boundary layer. In this work, the incoming boundary layer preceding the SBLI was measured $19.4\delta_0$ upstream of shock impingement (Fig. 6). The boundary-layer shape is consistent with fully developed, supersonic, turbulent velocity profiles, and the thickness agrees qualitatively with shadowgraph observations. The compressible displacement and momentum thicknesses are $0.27\delta_0$ and $0.075\delta_0$, respectively, as determined by the curve fit. The skin-friction coefficient c_f, also determined from the curve fit, is 1.34×10^{-3} for the incoming boundary layer.

The velocity profile closest to shock impingement ($x^* = -0.12$) clearly shows that this SBLI induces a separation bubble at least $0.1\delta_0$ in height. Other profiles obtained in the immediate vicinity of impingement document that the separation bubble begins at approximately $x^* = -2$ and persists a full boundary-layer thickness downstream of impingement.[21] The star locations in the centerline

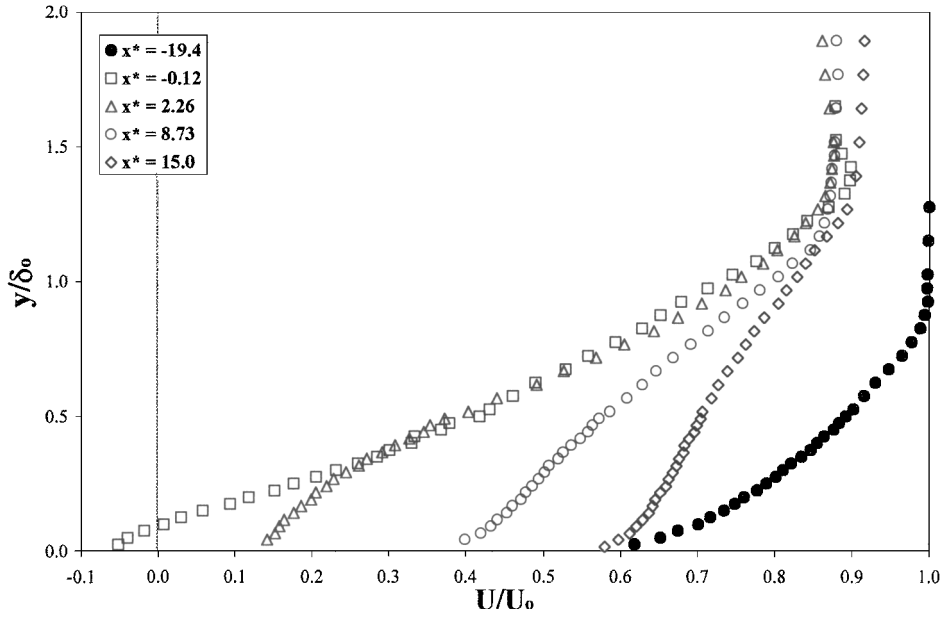

Fig. 6 Solid-wall boundary layer profiles at various streamwise locations.

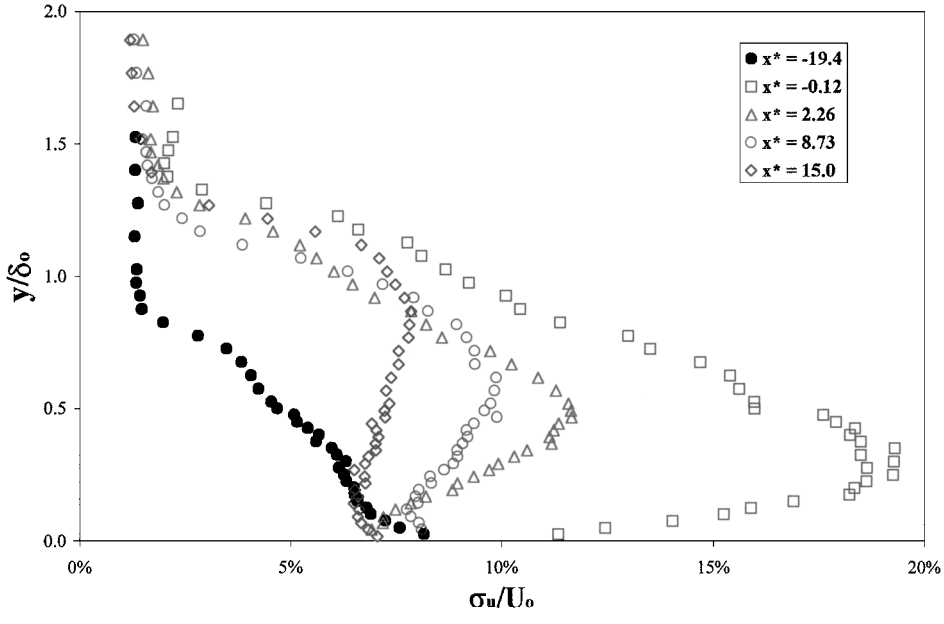

Fig. 7 Solid-wall streamwsie turbulence intensity profiles at various streamwise locations.

pressure profiles shown in Fig. 5 qualitatively reflect the location and extent of flow separation for the solid-wall case.

Generally, at each station after impingement, note that the boundary layer is much thicker and that the velocity profiles tend to have a semilinear shape over much of their extent, as compared to the incoming boundary layer. This observation has also been seen in computational results[20,30] and is attributed to wakelike behavior of the shear layer resulting from the preceding flow separation. The effect of the shock system on reducing the freestream velocity is seen at all stations at or beyond the impingement location. The velocity profile at $x^* = 2.26$ shows significant boundary-layerrecovery near the wall immediately after the SBLI.

Also note the presence of inflection points in the wake region (near $y/\delta_0 = 0.6$ and 0.9) for $x^* = 8.73$ and 15.0, respectively. These inflection points suggest an internal shear layer, which is further substantiated by the streamwise turbulence intensity profiles to be discussed subsequently. The profiles progressively become fuller downstream, but they do not reach fully developed equilibrium shapes even at a location $15\delta_0$ after shock impingement. Again, the velocity nearest the wall recovers faster than the rest of the wake region, as evidenced by the first inflection point close to the wall for the two downstreammost profiles.

The streamwise turbulence intensity, $\langle u'/U_0 \rangle = \sigma_U/U_0$, for the incoming and outgoing boundary layers are given in Fig. 7 for the same streamwise locations shown in Fig. 6. Note that the incoming boundary-layer turbulence intensity at $x^* = -19.4$ correlates well with earlier canonical turbulent boundary-layer distributions, that is, the maximum level of streamwise turbulence intensity is found closest to the wall, and the rms velocity fluctuation is somewhat less than 10% of the freestream velocity.[31] At shock impingement ($x^* = -0.12$), the peak streamwise turbulence intensity increases dramatically, reaching a level close to 20%, but at a higher transverse location ($y^* = 0.3$). This indicates the presence of an internal shear layer that persists until at least $15\delta_0$ downstream of impingement. The peak streamwise turbulence intensity steadily drops from 12% at $x^* = 2.26$ to around 7% at $15\delta_0$ downstream of shock impingement (and also shifts somewhat away from the wall), indicating gradual boundary-layer recovery.

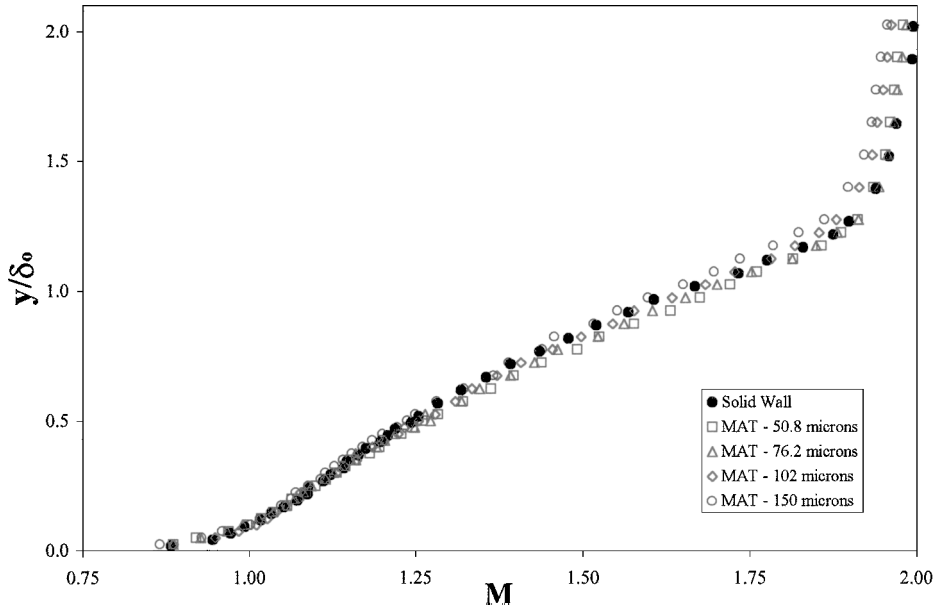

Fig. 8 Downstream boundary-layer Mach number profiles at $(x - x_0)/\delta_0 = 13.4$ for nitinol mesoflaps and baseline case.

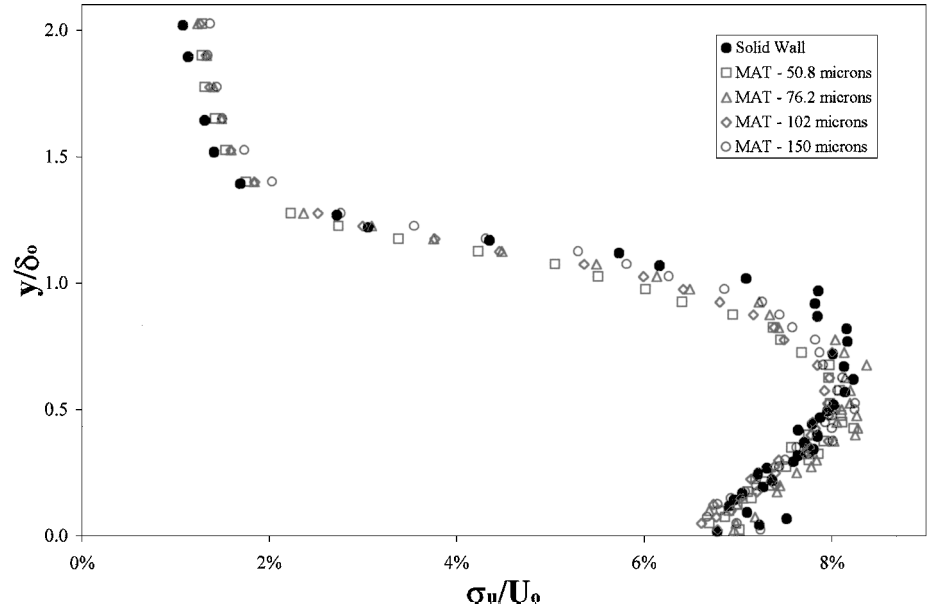

Fig. 9 Downstream boundary-layer streamwise turbulence intensity profiles at $(x - x_0)/\delta_0 = 13.4$ for nitinol mesoflaps and baseline case.

Nitinol Mesoflap Results

Velocity characteristics were measured at six stations downstream of the SBLI for the four different thicknesses of nitinol mesoflaps. These were converted to Mach number profiles to identify the portions of the flow that are supersonic and transonic. Figure 8 shows the boundary-layer Mach number profiles at $x^* = 13.4$ for the four nitinol flap thicknesses, along with the solid-wall results. The freestream Mach number increases slightly far from the wall as a result of the impinging expansion fan. Near the wall, the profiles all essentially collapse onto the solid-wall reference case, but then diverge in the wake region. The thickest mesoflap array shows a slight reduction in Mach profile fullness and a slight increase in boundary-layer thickness. The two thinnest flap arrays, however, show a similar overall boundary-layer thickness and a somewhat fuller mean Mach profile at y/δ_0 of about one (when compared to the no-bleed baseline).

Streamwise turbulence intensity profiles at the same streamwise location are presented in Fig. 9 for the same cases. All turbulence intensity contours peak at around $\sigma_U / U_0 = 8\%$, but the location of peak turbulence occurs at around $y/\delta_0 = 0.7$ for the solid-wall baseline and is at approximately $y/\delta_0 = 0.5$ for all mesoflap arrays. The solid-wall shear layer also appears to be thicker (as determined by the width of the turbulence intensity profiles) than for the mesoflap cases, presumably due to stronger upstream local shock interaction. The streamwise turbulence properties may be important in understanding and quantifying the overall degree of unsteadiness inherent in the interaction, as well as the potential capability for boundary-layer recovery. However, there does not appear to be significant variations in the magnitude or distribution of the turbulence intensity between the solid-wall case and the various mesoflap cases. Also, whereas spectra can not be derived from the ensembles of instantaneous velocity realizations of the LDV, it is known that the velocity probability density functions were approximately Gaussian in shape at every location with only one local maximum, even in the vicinity of shock impingement. This suggests that the shock did not exhibit macroscopic unsteadiness because bimodal probability distributions would result from this.

The fullness and magnitude of the stagnation pressure profile is an important consideration for supersonic inlets and was, thus, of interest herein. To avoid using intrusive techniques, LDV Mach number profiles were combined with the static pressure distributions to generate the approximate stagnation pressure profile from the isentropic

pressure ratio relation. This assumes little or no curvature of the streamlines and no compression or expansion waves in the region of interest, which is only reasonably satisfied at $(x - x_0)/\delta_0 = 8.73$ out to 9.5 mm above the wall ($y/\delta_0 = 2.4$), before encountering the effects of the expansion fan/Mach wave interaction. The ratio of post- to preinteraction stagnation pressures is shown in Fig. 10, where several important features can be noted, especially when compared with the experimental stagnation pressure profiles of McCormick.[15] First, the baseline stagnation pressure ratio begins at 0.2 near the wall and increases sharply in the range $y/\delta_0 = 1.0 \pm 0.25$. It reaches a constant value ($P_t/P_0 = 0.955$) at $y/\delta_0 = 1.75$ (corresponding to streamlines that have passed through the leading shock system) and then decreases slightly to a new value of $P_t/P_0 = 0.94$ around $y/\delta_0 = 2.15$ (corresponding to flow that passed through the incident and reflected shocks). In comparison, the inviscid stagnation pressure recovery is 0.983 (based on two oblique shocks reflecting due to a pair of 8-deg turns and a Mach 2.41 initial flow). The variations between experimentally observed and theoretical (inviscid) stagnation pressure ratio observed in this study for the solid-wall case are similar to those observed by McCormick,[15] for which the experimental ratio was 0.69 and the theoretical ratio was 0.77. Likewise, oblique SBLI studies by Reda and Murphy[32] found an experimental value of about 0.78 for an inviscid recovery of 0.82.

The nitinol flaps of 50.8- and 76.2-μm thicknesses show improved stagnation pressure recovery over the baseline no-bleed case, with the thinnest array yielding the greatest improvement. The thickest array (150 μm) yielded the poorest pressure recovery, ostensibly due to the lack of flap deflection and the resulting nearly normal injection and bleed. Similarly, the 102-μm nitinol mesoflaps deflected only a very slight amount and showed a moderate improvement in pressure recovery compared to the thickest array. For all passive control cases, the stagnation pressure ratio values continue to increase up to the furthest measurement location from the wall. Because the passive mesoflap control diffuses the SBLI, the resulting stagnation

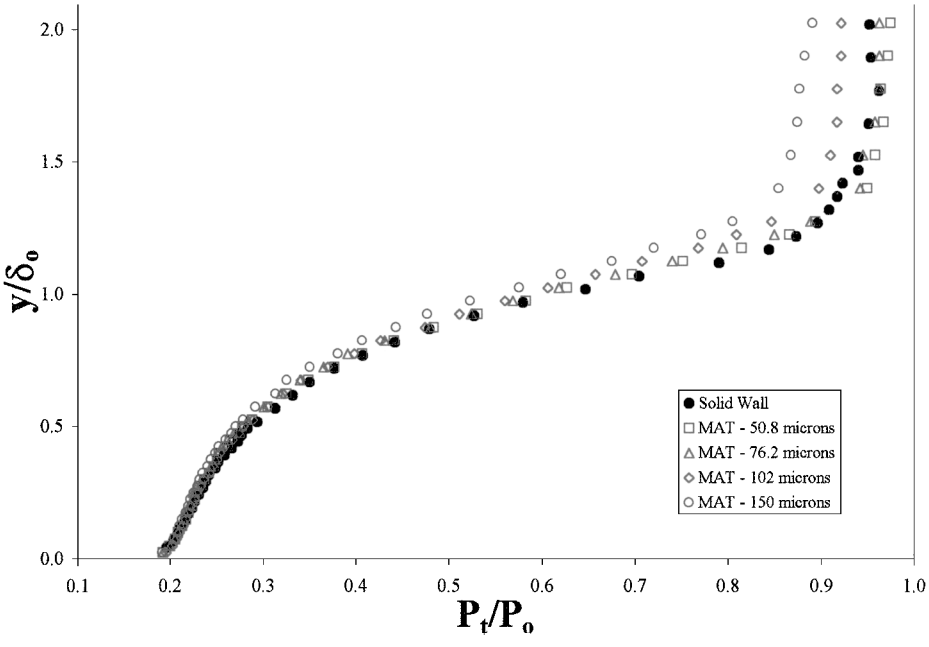

Fig. 10 Downstream boundary-layer stagnation pressure profiles at $(x - x_0)/\delta_0 = 8.73$ for nitinol mesoflaps and baseline case.

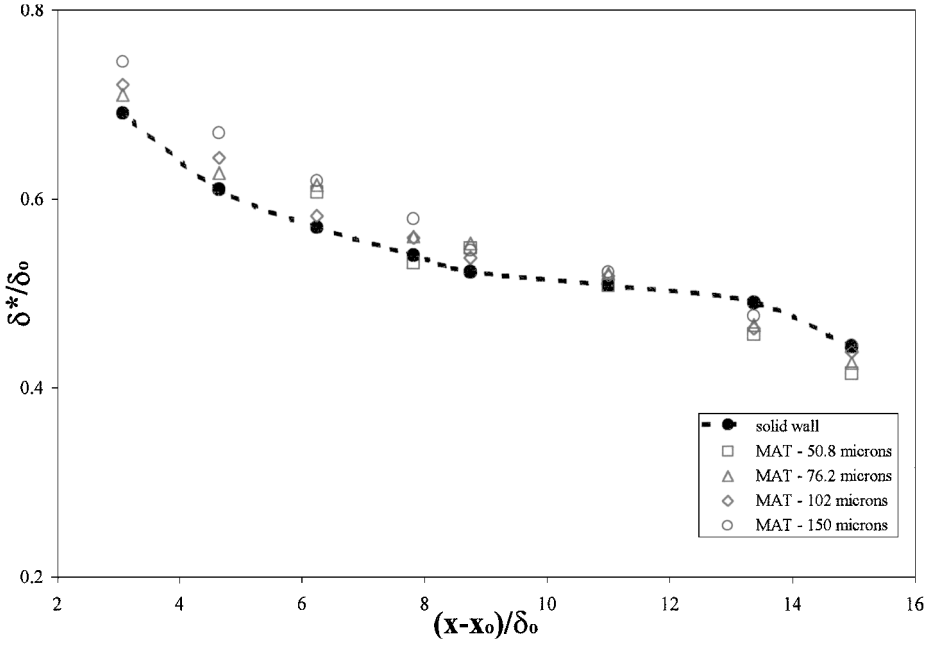

Fig. 11 Downstream boundary-layer displacement thickness evolution for nitinol mesoflaps and baseline case.

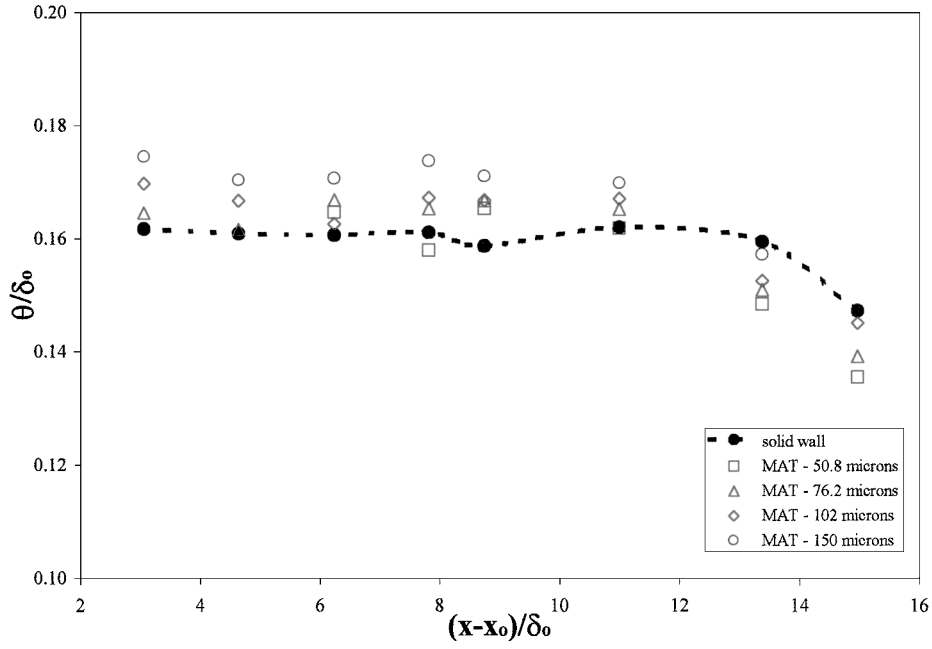

Fig. 12 Downstream boundary-layer momentum thickness evolution for nitinol mesoflaps and baseline case.

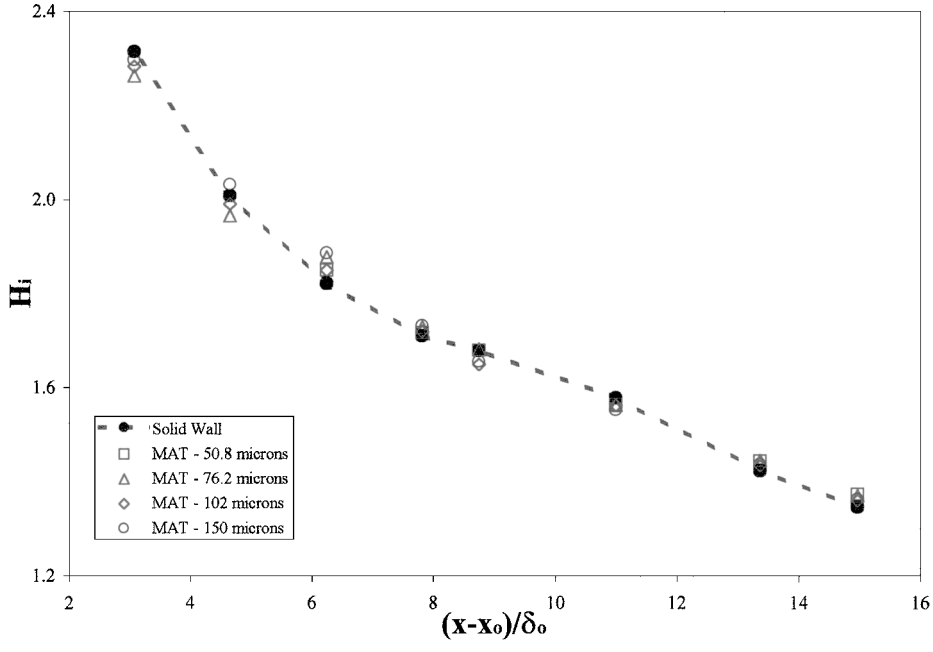

Fig. 13 Downstream boundary-layer incompressible shape factor evolution for nitinol mesoflaps and baseline case.

pressure recovery reaps more of what McCormick[15] termed the "lambda-foot benefit." The thinnest mesoflaps show the greatest benefit, partly due to the higher downstream static pressure recovery. This is even more marked further downstream,[21] although this region includes wave interactions that render the stagnation pressure profiles qualitative only. For normal shock control, McCormick[15] found that a porous surface and a passive cavity provided much poorer pressure recovery near the wall compared to the baseline case, whereas a series of vortex generators (which significantly reduced the boundary-layer thickness) provide improved pressure recovery close to the wall. Although the changes in stagnation pressure obtained with the thinnest mesoflap arrays are not dramatic, note that a stagnation pressure increase of just 1% in the subsonic diffuser of a supersonic inlet is considered to be desirable and significant. However, the present measurements are limited to both the spanwise centerline portion of the flow and to a supersonic region immediately downstream of the interaction, such that no definitive conclusion can be made regarding the overall performance for inlet-type operation.

At all stations downstream of the SBLI, boundary-layer parameters were calculated from the LDV data and are presented as a function of streamwise distance in Figs. 11–13. The incompressible boundary-layer characteristics (δ^*, θ, and H_i) were calculated directly from the experimental data. Figure 11 shows the boundary-layer displacement thickness for the solid-wall reference case, along with the nitinol mesoflaps, where the thickest array yields the largest downstream displacement thickness. However, as was observed in the Mach number and stagnation pressure profiles, the two thinnest arrays typically yield the best reduction in δ^* of all nitinol mesoflaps. For $x^* > 12$, nearly all mesoflap thicknesses outperform the no-bleed baseline, especially the 50.8-μm array, which shows nearly a 7% reduction in displacement thickness over the solid wall $13.4\delta_0$ downstream of impingement. Note that the data near the cavity center, for example, $x^* = 2.8$, show that the displacement thickness for

all of the mesoflaps is greater than the solid-wall case. This suggests that mass injection through the upstream flaps is generally not favorable to boundary-layer health but that the resulting downstream bleed offsets this loss to some degree. Such a hypothesis is consistent with previous studies of boundary-layer bleed (for which there is no upstream injection). Thus, for the thinnest flaps, the benefits of the downstream bleed may supercede the deleterious effects of the upstream injection to yield a net overall improvement as compared to the solid-wall baseline.

Similar trends are apparent in Fig. 12, where the normalized momentum thickness is plotted as a function of downstream distance. Once again, the thickest array has a deleterious impact on the momentum thickness at all stations preceding expansion fan impingement. The momentum thickness was reduced considerably at the two most downstream boundary-layer measurement locations with the nitinol arrays, particularly for the thinnest flaps. At $13.4\delta_0$ downstream of impingement, the 76.2- and 50.8-μm arrays reduced the momentum thickness over the no-bleed baseline by 5.4 and 6.9%, respectively. Such variations can be significant, but are smaller than the reductions typically noted with conventional bleed systems.[5]

Because there were similar levels of reduction of the displacement and momentum thicknesses, the incompressible shape factor was found to be nearly identical to the solid-wall baseline for all mesoflap arrays, as shown in Fig. 13. Although the two stations farthest upstream (3.1 and $4.6\delta_0$) do show a minor improvement in shape factor for the thinnest mesoflaps, the shape factor for all cases is equal to 1.35 (close to the equilibrium value of 1.3) at the end of the measurement domain.

Conclusions

An experimental investigation of aeroelastic mesoflaps to provide recirculating transpiration to control oblique SBLIs has been conducted. Experiments were performed in a Mach 2.45 wind tunnel to verify the applicability of the mesoflap concept for controlling oblique SBLIs; experiments included shadowgraph flow visualizations, surface pressure measurements, and LDV measurements along the spanwise midplane.

The shadowgraphs of the solid-wall (no-bleed) baseline study revealed the typical features of an oblique SBLI, including significant boundary-layer growth after impingement, and a leading shock caused by flow separation. With the mesoflap system installed, the upstream flow injection and angled bleed downstream significantly altered the entire flowfield. In particular, the leading shock was always generated at the first flap, thereby diffusing the shock footprint. At impingement, the boundary layer (as compared to the solid-wall case) was qualitatively thicker for the mesoflap cases due to the upstream flow injection. However, due to the bleed region of the mesoflaps, the downstream boundary-layer growth was qualitatively reduced, such that, in the case of the thinnest (most effective) flaps, the outgoing boundary-layer thickness was similar to the solid-wall case. Based on the LDV measurements, the thinnest mesoflap arrays showed evidence of reduced boundary-layer displacement thickness and momentum thickness downstream of the interaction as compared to the solid-wall case (and as compared to the thicker mesoflaps). Similarly, static and approximate stagnation pressure profiles showed somewhat better pressure recovery downstream of the SBLI for the mesoflap arrays with the largest deflections, that is, thinnest flaps, as compared to either the solid-wall case or the thicker mesoflaps.

In general, the present results suggest that the upstream injection limits the recirculation performance. There are several possible remedies that may correct this problem: 1) Inject the recirculating flow over a greater streamwise distance (more flaps upstream) to lower the local injection velocities. 2) Test a hybrid approach, using a microporous skin for upstream injection and mesoflaps for downstream bleed, whereby both injection velocity and deflection are reduced. 3) Use fixed-geometry, high-speed tangential injection to energize the low-momentum portion of the boundary layer near the wall. 4) Utilize active flap control to increase the stiffness of upstream flaps to limit their deflection. 5) Move the upstream flaps further from the interaction region. However, many other issues remain concerning the evaluation of this concept. For example, detailed comparison to conventional (and successful) bleed methods, effects of three dimensionality, subsonic diffuser performance, and the influence on skin friction should be considered in future studies.

Acknowledgments

This work was supported under Contract F49620-98-1-0490 by the Defense Advanced Research Projects Agency, with Richard Wlezien as Technical Monitor, and the Air Force Office of Scientific Research, with Steven Walker as Technical Monitor.

References

[1]Delery, J., and Bur, R., "Shock Wave/Boundary Layer Interaction and Control Techniques: A Physical Description," 22nd International Symposium on Shock Waves, Paper 6010, July 1999.

[2]Delery, J. M., "Experimental Investigation of Turbulence Properties in Transonic Shock/Boundary-Layer Interactions," *AIAA Journal*, Vol. 21, No. 2, 1983, pp. 180–185.

[3]Settles, G. S., and Dodson, L. J., "Supersonic and Hypersonic Shock/Boundary-Layer Interaction Database," *AIAA Journal*, Vol. 32, No. 7, 1994, pp. 1377–1383.

[4]Hamed, A., and Kumar, A., "Flow Separation in Shock Wave Boundary Layer Interactions," *Journal of Engineering for Gas Turbines and Power*, Vol. 116, Jan. 1994, pp. 98–103.

[5]Hamed, A., Yeuan, J. J., and Shih, S. H., "Shock-Wave/Boundary-Layer Interactions with Bleed. Part 1: Effect of Slot Angle," *Journal of Propulsion and Power*, Vol. 11, No. 6, 1995, pp. 1231–1235.

[6]Donovan, J. F., "Control of Shock Wave/Turbulent Boundary Layer Interactions Using Tangential Injection," AIAA Paper 94-0443, Jan. 1994.

[7]Stanwesky, E., Delery, J., Fulker, J., and Geibler, W., "EUROSHOCK—Drag Reduction by Passive Shock Control," *Notes on Numerical Fluid Mechanics*, Vol. 56, 1997, pp. 50–75.

[8]Bahi, L., "Passive Shock Wave/Boundary Layer Control for Transonic Supercritical Airfoil Drag Reduction," Ph.D. Dissertation, Dept. of Mechanical, Aerospace and Nuclear Engineering, Rensselaer Polytechnic Inst., Troy, NY, 1982.

[9]Bahi, L., Ross, J. M., and Nagamatsu, H. T., "Passive Shock Wave/Boundary Layer Control for Transonic Airfoil Drag Reduction," AIAA Paper 83-0137, Jan. 1983.

[10]Loth, E., "Smart Mesoflaps for Control of Shock Boundary-Layer Interactions," AIAA Paper 2000-2476, June 2000.

[11]Raghunathan, S., "Passive Control of Shock Boundary Layer Interaction," *Progress in Aerospace Science*, Vol. 5, 1988, pp. 271–296.

[12]Raghunathan, S., and McIlwain, S. T., "Further Investigations of Transonic Shock-Wave/Boundary-Layer Interaction with Passive Control," *Journal of Aircraft*, Vol. 27, No. 1, 1990, pp. 60–65.

[13]Bur, R., Delery, J., Corbel, B., Soulevant, D., and Soares, R., "A Basic Experimental Investigation of Passive Control Applied to a Transonic Interaction," *Aerospace Science and Technology*, Vol. 2, No. 1, 1998, pp. 61–73.

[14]Bur, R., Corbel, B., and Delery, J., "Study of Passive Control in a Transonic Shock-Wave/Boundary-Layer Interaction," *AIAA Journal*, Vol. 36, No. 3, 1998, pp. 394–400.

[15]McCormick, D. C., "Shock/Boundary-Layer Interaction Control with Vortex Generators and Passive Cavity," *AIAA Journal*, Vol. 31, No. 1, 1993, pp. 91–96.

[16]Gibson, T. M., Babinsky, H., and Squire, L. C., "Passive Control of Normal Shock-Wave/Turbulent Boundary-Layer Interaction," 21st International Symposium on Shock Waves, Paper 1220, July 1997.

[17]Rolston, S., and Raghunathan, S., "Passive Control of Pre-entry Shock in Supersonic Intakes," AIAA Paper 93-0291, Jan. 1993.

[18]Laurendeau, E., "Boundary-Layer Bleed Roughness," Ph.D. Dissertation, Dept. of Aeronautics and Astronautics, Univ. of Washington, Seattle, WA, 1995.

[19]Lin, Y. L., Rimlinger, M. J., Shih, T. I. P., and Willis, B. P., "Control of Shock-Wave/Boundary-Layer Interactions with Passive Blowing and Bleeding," AIAA Paper 97-3002, July 1997.

[20]Wood, B., Loth, E., and Geubelle, P., "Mesoflaps for Aeroelastic Transpiration for SBLI Control," AIAA Paper 99-0614, Jan. 1999.

[21]Gefroh, D. L., "Experimental Study of Mesoflaps to Control Oblique-Shock/Boundary-Layer Interaction," M.S. Thesis, Dept. of Aeronautical and Astronautical Engineering, Univ. of Illinois, Urbana, IL, June 2000.

[22]Carroll, B. F., and Dutton, J. C., "Turbulence Phenomena in a Multiple Normal Shock Wave/Turbulent Boundary-Layer Interaction," *AIAA Journal*, Vol. 30, No. 1, 1992, pp. 441–448.

[23]Palko, C. W., and Dutton, J. C., "A Method for Separating Shock Wave Motion and Turbulence in LDV Measurements," *Experiments in Fluids*, Vol. 26, No. 4, 1999, pp. 358–370.

[24]Bloomberg, J. E., "An Investigation of Particle Dynamics Effects Related to LDV Measurements in Compressible Flows," M.S. Thesis, Dept. of Mechanical and Industrial Engineering, Univ. of Illinois, Urbana, IL, 1989.

[25]Amatucci, V. A., "An Experimental Investigation of the Two-Stream, Supersonic, Near-Wake Flowfield Behind a Finite-Thickness Base," Ph.D. Dissertation Dept. of Mechanical and Industrial Engineering, Univ. of Illinois, Urbana, IL, 1990.

[26]Seddon, J., "The Flow Produced by the Interaction of a Turbulent Boundary Layer with a Normal Shock Wave of Strength Sufficient to Cause Separation," Aeronautical Research Council, R&M 3502, March 1960.

[27]Squire, L. C., "A Review of the Role of Some Small High-Speed Wind Tunnels in Aeronautical Research," *Progress in Aerospace Sciences*, Vol. 34, 1998, pp. 107–166.

[28]Porro, A. R., and Hingst, W. R., "Use of Surface Heat Transfer Measurements as a Flow Separation Diagnostic in a Two-Dimensional Reflected Oblique Shock/Turbulent Boundary Layer Interaction," AIAA Paper 93-0775, Jan. 1993.

[29]Sun, C. C., and Childs, M. E., "Modified Wall Wake Velocity Profile for Turbulent Compressible Boundary Layers," *Journal of Aircraft*, Vol. 10, No. 6, 1973, pp. 381–383.

[30]Wood, B., Loth, E., Geubelle, P., and McIlwain, S. T., "A Numerical Methodology for an Aeroelastic SBLI Flow," AIAA Paper 2000-0552, Jan. 2000.

[31]Klebanoff, P. S., "Characteristics of Turbulence in a Boundary Layer with Zero Pressure Gradient," NACA Rept. 1247, 1955.

[32]Reda, D. C., and Murphy, J. D., "Shock Wave/Turbulent Boundary Layer Interaction in Rectangular Channels" *AIAA Journal*, Vol. 11, No. 2, 1973, pp. 139, 140.

M. Sichel
Associate Editor